Journal of Electronic Materials (2022) 51:6637–6644
https://doi.org/10.1007/s11664-022-09975-z

TOPICAL COLLECTION: ADVANCED METAL ION BATTERIES

Confined Synthesis of SnO_2 Nanoparticles Encapsulated in Carbon Nanotubes for High-Rate and Stable Lithium-Ion Batteries

Ying Liu[1] · Ling Chen[2] · Hao Jiang[1,2] · Chunzhong Li[1,2]

Received: 28 July 2022 / Accepted: 15 September 2022 / Published online: 13 October 2022

Abstract

The use of tin oxide (SnO_2) with high theoretical capacity in practical application as the anode material of lithium-ion batteries (LIBs) has been limited due to its large volume expansion and fast capacity decay. To address this problem, we proposed the synthesis of encapsulating SnO_2 nanoparticles in the channels of nitrogen-doped carbon nanotubes (SnO_2-in-NCNTs) by capillary force. The confined spaces of NCNTs not only restrict the particle size of SnO_2, but also effectively buffer the volume change during lithiation/delithiation processes. In addition, the conductive NCNTs also ensure the effective contact of the electrolyte to the electrode surface, facilitating both ion and electron transfer. When applied to LIBs, the SnO_2-in-NCNTs possess high reversible capacities of 961.8 mAh g^{-1} at 0.1 A g^{-1} and 326.3 mAh g^{-1} at 10 A g^{-1}. Moreover, they exhibited superior cyclic stability with a capacity retention of 96% at 5 A g^{-1} after 500 cycles. This work provides a simple and effective strategy for performance improvement of SnO_2-based anode materials.

Keywords Lithium-ion batteries · SnO_2 · carbon nanotubes · confined synthesis

Introduction

Lithium-ion batteries (LIBs) are the predominant energy storage devices in modern portable electronic devices and electric vehicles. However, the traditional graphite anodes which are limited by a low theoretical capacity of 372 mAh g^{-1} cannot satisfy the next-generation LIBs with higher energy and power densities.[1–3] Various alternative materials with high reversible capacity, including metals, alloys, and metallic oxides/sulfides, have been investigated extensively.[4–8] Among them, tin oxide (SnO_2) has attracted great attention in view of its abundance, high theoretical capacity (1494 mAh g^{-1}) and low working potential.[9–11] Nevertheless, the practical application of SnO_2 anode in LIBs is still impeded by its inherent disadvantages. For instance, the severe pulverization and serious capacity fading due to large volume expansion (> 300%) during lithiation/delithiation processes lead to rapid capacity fading. In addition, the SnO_2 with poor conductivity is not conducive to electron transmission, which results in poor rate performance.[12–15]

To conquer these defects, reducing the size of SnO_2 can relieve the mechanical stress and thus inhibit the tendency to fracture and crack.[16,17] Furthermore, such design will generally promote the high reversibility and realize the long cycling stability of SnO_2. Despite partial problems that can be solved, the intrinsic low conductivity of SnO_2 still exists. One effective strategy is to combine nanoscale SnO_2 with an electrically conductive carbonaceous matrix. Among these carbon materials, carbon nanotubes (CNTs) have received wide attention due to their high electrical conductivity, large surface area and mechanical stability.[18–21] Liu et al.[22] synthesized SnO_2/carbon nanotube hairball composites with SnO_2 nanoparticles homogeneously anchored on the surface of CNTs, achieving high lithium storage properties and an excellent high-rate capability. However, the SnO_2 nanoparticles inevitably fall off from CNTs during long cycles, resulting in deterioration of the electrochemical performance.

✉ Ling Chen
chenling@ecust.edu.cn

✉ Hao Jiang
jianghao@ecust.edu.cn

[1] Key Laboratory for Ultrafine Materials of Ministry of Education, School of Materials Science and Engineering, East China University of Science and Technology, Shanghai 200237, China

[2] Shanghai Engineering Research Center of Hierarchical Nanomaterials, School of Chemical Engineering, East China University of Science and Technology, Shanghai 200237, China

Embedding SnO_2 nanoparticles into carbon nanotubes is a potential solution to solve such problems. Previous studies have proved that the wet chemical method utilizing the capillary force is a convenient method to achieve such a structure.[23–25] The capillary effect mainly depends on the inner diameter of CNTs and surface tension. Guo et al.[26] proved that the addition of polyvinylpyrrolidone (PVP) could decrease the surface tension, thus increasing the effect of capillary action to fill the inner hollow cavities with GeO_2/NaCl in an aqueous solution. Therefore, PVP is expected to be applied to the filling of commercial CNTs with solution.

Herein, we propose a simple strategy to synthesize the SnO_2 nanoparticles encapsulated in CNTs by capillary force. The results reveal that PVP can effectively reduce surface tension of the PVP/ethanol solution, which is conducive to solution filling in CNTs. Finally, the SnO_2/nitrogen-doped carbon nanotubes (SnO_2-in-NCNTs) were obtained after a two-step calcination. The conductive NCNTs ensure the effective contact of the electrolyte to the electrode surface, facilitating both ion and electron transfer. In addition, the confined space of NCNTs restricts the particle size of SnO_2. Moreover, there are sufficient void spaces between the adjacent particles in the NCNTs, which can accommodate the volume change of SnO_2 during the lithiation/delithiation processes. Consequently, the resulting SnO_2-in-NCNTs exhibit enhanced cycling stability (483.6 mAh g^{-1} after 500 cycles at 5 A g^{-1}) and better rate performance (326.3 mAh g^{-1} at 10 A g^{-1}) in comparison with SnO_2 nanoparticles dispersed on the surface of the same CNTs (SnO_2-out-NCNTs).

Experimental

Materials

Multiwalled carbon nanotubes with 5–10 nm inner diameter were purchased from Aladdin, polyvinylpyrrolidone (PVP, $M_W = 10{,}000$) was purchased from Adamas, stannous chloride dihydrate ($SnCl_2{\cdot}2H_2O$, 99%) was purchased from Adamas, and absolute ethanol (EtOH, ≥ 99.7%) was purchased from Greagent. All the chemicals and reagents were used without any further processing.

Synthesis of SnO_2-in-NCNTs, SnO_2-out-NCNTs, SnO_2-in-CNTs

Typically, 100 mg of CNTs and 30 mg of PVP were dispersed in 100 mL of absolute ethanol. After sonication for 1 h, 40 g of $SnCl_2{\cdot}2H_2O$ was added into the above solution and stirred for 10 h. The mixture was further filtered and washed with ethanol solution. Then, the precipitates were dried in an oven at 60°C for 12 h. Subsequently, the dried precipitates were pyrolyzed in a tube furnace at 400°C for 2 h under Ar atmosphere (ramp rate: 5°C min^{-1}), and then heated under 500°C in NH_3 atmosphere and maintained for 0.5 h. Afterwards, the system was naturally cooled to room temperature, forming the product of SnO_2-in-NCNTs. As a control, the SnO_2-out-NCNTs were prepared by the same process without addition of PVP, while the SnO_2-in-CNTs were obtained without the subsequent NH_3 atmosphere annealing compared with the preparing processes of SnO_2-in-NCNTs.

Characterization

The morphology and structure of the samples were characterized with a field-emission scanning electron microscope (SEM, FEI Nova NanoSEM 450) and a transmission electron microscope (TEM, FEI Talos F200s). X-ray diffraction (XRD) was analyzed by Bruker D8 Advance x-ray powder diffractometer using Cu Kα ($\lambda = 0.154$ nm) radiation operated at 40 kV and 40 mA. The content of SnO_2 in the composites was determined by thermogravimetric (TG) analysis on a Netzsch STA449F5 simultaneous thermal analyzer. The ex situ Raman spectra were obtained by an iHR550 Raman microscope with a 532-nm laser. Brunauer–Emmett–Teller (BET) specific surface area was obtained from N_2 isotherms by using a Micromeritics ASAP 2010 analyzer. X-ray photoelectron spectroscopy (XPS) was performed with a Thermo Scientific EscaLab 250Xi spectrometer using an Al Kα x-ray source ($h\nu = 1468.6$ eV) to detect the surface chemical states. The oxygen vacancy concentration was characterized using electron paramagnetic resonance (EPR) was obtained on a 100G-18 KG/EMX-8/2.7 (Bruker).

Electrochemical Measurements

To prepare the working electrodes, 80% active material, 10% carbon black and 10% poly(vinyldifluoride) were homogeneously mixed in N-methyl-2-pyrrolidinone solvent. Then, the resultant slurry was uniformly coated on Cu foil and dried at 120°C for 12 h under vacuum conditions. The loading of active materials is 0.8—1 mg cm^{-2} and the electrochemical properties of the as-prepared electrodes were measured using coin-cell batteries (CR2016) assembled in an Ar-filled glove box with lithium foil as the counter electrode and polypropylene membrane (Celgard 2400) as the separator. The electrolyte was 1 M $LiPF_6$ (1 M) in a mixture of ethylene carbonate (EC)/diethyl carbonate (DEC) (1:1 in volume)/5 wt% fluoroethylene carbonate (FEC). The cycled electrodes were first washed by DMC solvent and then dried at 100°C for 2 h for characterization. Galvanostatic charge–discharge experiments were conducted in the voltage range of 0.01 to 3 V (vs. Li^+/Li) by a LAND CT2001A battery tester over a series of specific current densities at room temperature. The cyclic voltammetry (CV) measurements (at various

scanning rates from 0.2 to 1.0 mV s^{-1}) and electrochemical impedance spectroscopy (EIS) over a frequency range from 100 kHz to 0.01 Hz were obtained with an Autolab PGSTAT302N electrochemical workstation.

Results and Discussion

Figure 1 schematically illustrates the synthesis of SnO_2-in-NCNTs via the wet chemistry method. Typically, the PVP was first introduced into the ethanol solution with CNTs evenly dispersed to reduce the surface tension and thus ensure the adequate wettability of CNTs. The $SnCl_2 2H_2O$ was then added into the above solution with constant stirring, and the $SnCl_2$/PVP mixed solution was infiltrated into the tube of CNTs through capillary force. Finally, the as-prepared precursor was pyrolyzed by a two-step process in a tube furnace to obtain the SnO_2-in-NCNTs. During the annealing process under an NH_3 atmosphere, the CNTs were doped with nitrogen successfully. As a control, the SnO_2-out-NCNTs were prepared by the same processes just without the addition of PVP. In order to clarify the role of PVP in the solution, the solution tension of pristine ethanol and the ethanol solution with PVP were measured. As shown in Fig. S1, the PVP can effectively reduce surface tension of the PVP/ethanol solution, which similarly is conducive to the solution filling in NCNTs. It is obvious that the PVP plays a key role in the capillary force enhancement.

The morphology and microstructure of as-prepared SnO_2-in-NCNTs and SnO_2-out-NCNTs were characterized by SEM and TEM. As shown in Fig. 2a, SnO_2-in-NCNTs show a smooth surface of NCNTs while the SnO_2-out-NCNTs show clustered nanoparticles attached to the external surfaces of NCNTs (Fig. 2b). The TEM images of SnO_2-in-NCNTs are subsequently presented in Fig. 2c-d. Figure 2c shows that the morphology of commercial NCNTs is still well retained and the channels of NCNTs are filled with aligned nanoparticles (~5 nm). High-resolution TEM (Fig. 2d) reveals that the lattice spacing of the particles is 0.34 nm, which is assigned to the SnO_2 (110) plane, as is further validated in the fast Fourier transform (FFT) image (inset of Fig. 2c).[9] Nevertheless, as shown in Fig. S2, most of the SnO_2 nanoparticles in SnO_2-out-NCNTs are dispersed on the outside of the NCNTs with larger grain diameter.

Typical XRD patterns of the SnO_2-in-NCNTs and SnO_2-out-NCNTs are shown in Fig. 3a. The diffraction peaks for two samples match well with SnO_2 (PDF #41–1445).[27] The mass content of SnO_2 in the two hybrids are both calculated to ~ 58 wt% based on the TG analysis (Fig. 3b). Furthermore, the XPS was studied to investigate the chemical bonding of the two as-synthesized samples. Figure S3a presents the survey XPS spectra of SnO_2-in-NCNTs and SnO_2-out-NCNTs, suggesting the presence of Sn, O, C and N. In the Sn 3d spectra (Fig. S3b) of the two hybrids, two peaks at 487.1 eV and 495.6 eV belong to Sn $3d_{5/2}$ and Sn $3d_{3/2}$, which suggests the presence of Sn^{4+} in the SnO_2. The C1s spectrum of SnO_2-in-NCNTs can be fitted into three peaks (Fig. 3c), among which the peaks at 284.8 eV and 288.8 eV correspond to C–C/C = C and O = C–OH, respectively. Another peak at 286.1 eV belongs to Sn–O-C, which is considered beneficial for keeping a highly stable structure during cycle processes.[28] The C 1s spectrum of SnO_2-out-NCNTs is provided in Fig. S4, and the weaker Sn–O-C bond is shown in SnO_2-in-NCNTs which indicates an inferior connection of SnO_2 and NCNTs. The nitrogen content is 2.1% according the XPS analysis and the N 1s XPS spectrum of SnO_2-in-NCNTs can be resolved into pyridinic N, pyrrolic N and graphitic N, respectively, centered at 398.5 eV, 399.9 eV and 401.1 eV (Fig. S5).[29] The N_2 isotherms and pore size distribution are shown in Fig. 3d, and obvious type-H_3 hysteresis rings can be observed when the relative pressure P/P_0 is high. The specific surface area of SnO_2-in-NCNTs (87.9 m^2 g^{-1}) is lower than SnO_2-out-NCNTs (132.1 m^2 g^{-1}) owing to homogeneous filling of the ultrafine SnO_2 nanoparticles into NCNTs. EPR analysis was performed on the two samples (Fig. S6), and

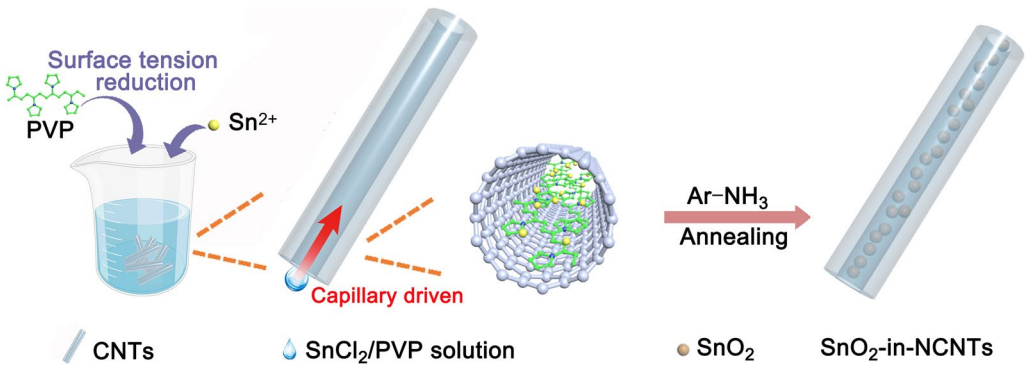

Fig. 1 Schematic diagram of the fabrication process of the SnO_2-in-NCNTs.

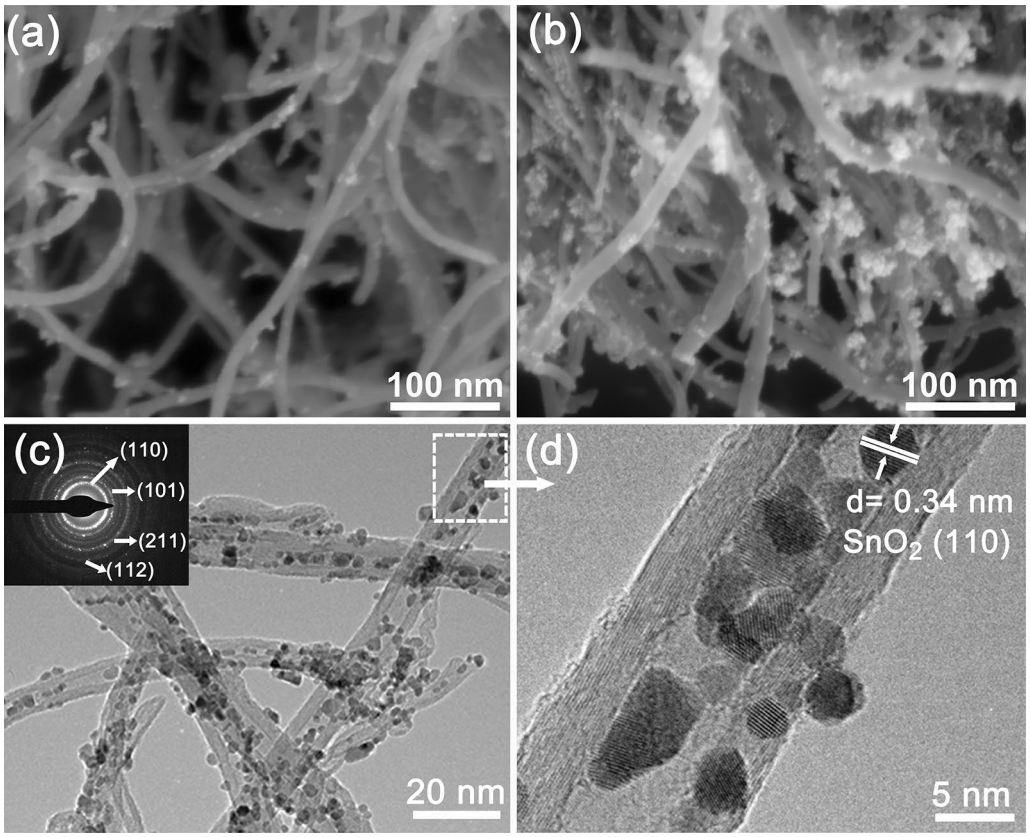

Fig. 2 SEM images of (a) SnO_2-in-NCNTs and (b) SnO_2-out-NCNTs. (c) Low- and (d) high-magnification TEM images of SnO_2-in-NCNTs.

both of the EPR spectra present EPR activity, proving the presence of an oxygen vacancy (V_O), which is an effective way to improve the Li^+ storage kinetics.[27,30–32]

The as-prepared hybrids were evaluated as anode materials for LIBs, and the electrochemical performance of cyclic voltammetry was first evaluated. According to Fig. 4a and b, there are two reduction peaks for SnO_2-in-NCNTs and SnO_2-out-NCNTs in the first cathodic scan. The reduction peak at ~ 0.8 V is related to the formation of SEI film and the conversion reaction of SnO_2 to Sn and Li_2O.[33–35] The peak around 0.1 V is due to the formation of Li_xSn alloy. There are three oxidation peaks at ~ 0.49, 1.2 and 1.85 V in the first delithiation stage. The oxidation peak at ~ 0.52 V is the dealloying reaction of SnO_2. The peaks at ~ 1.26 and 1.84 V correspond to the conversion reaction from Sn to SnO_2, respectively. An additional oxidation peak at ~ 2.49 V is observed in the SnO_2-in-NCNTs, indicating its higher reversibility. The initial three charge–discharge profiles of the SnO_2-in-NCNTs, SnO_2-out-NCNTs at current density of 0.1 A g^{-1} with voltage range from 0.01 to 3.0 V are presented in Fig. S7. Obviously, the electrochemical behavior is consistent with that observed on the CV curves. The obtained specific charge capacity of SnO_2-in-NCNTs is 961.8 mAh g^{-1} with higher coulombic efficiency (68.7%), which is higher than SnO_2-out-NCNTs (833.2 mAh g^{-1}, 58.3%). Furthermore, the advantage of nitrogen doping can be verified by comparing with undoped sample (SnO_2-in-CNTs). The rate performance was evaluated for all samples at 0.1 A g^{-1}, 0.2 A g^{-1}, 0.5 A g^{-1}, 1 A g^{-1}, 2 A g^{-1}, 5 A g^{-1} and 10 A g^{-1}. the SnO_2-in-NCNTs performs the best at any rate (Fig. 4c). More impressively, after high-current density measurement, the capacity of the SnO_2-in-NCNTs can recover to its initial value at 0.1 A g^{-1}, indicating a high reversibility of the composite. The capacity contribution of SnO_2 is calculated under various current densities (Fig. 4d, Fig. S9). For example, in the first cycle the capacity of SnO_2 can be calculated to 1412.1 mAh g^{-1} in SnO_2-in-NCNTs according to the capacity contribution of NCNTs (Fig. S8), which is almost equal to the theoretical capacity of SnO_2 and much higher than 1249.8 mAh g^{-1} in SnO_2-out-NCNTs. Furthermore, the capacity contributed by SnO_2 in SnO_2-out-NCNTs decays rapidly with increasing current density. The EIS of SnO_2-in-NCNTs, SnO_2-in-CNTs and SnO_2-out-NCNTs before cycling are provided in Fig. S10. The charge transfer resistance (Rct) of SnO_2-in-NCNTs is smaller than that of SnO_2-out-NCNTs and SnO_2-in-CNTs, indicating the higher charge transfer and good electrical conductivity of SnO_2-in-NCNTs.[36,37]

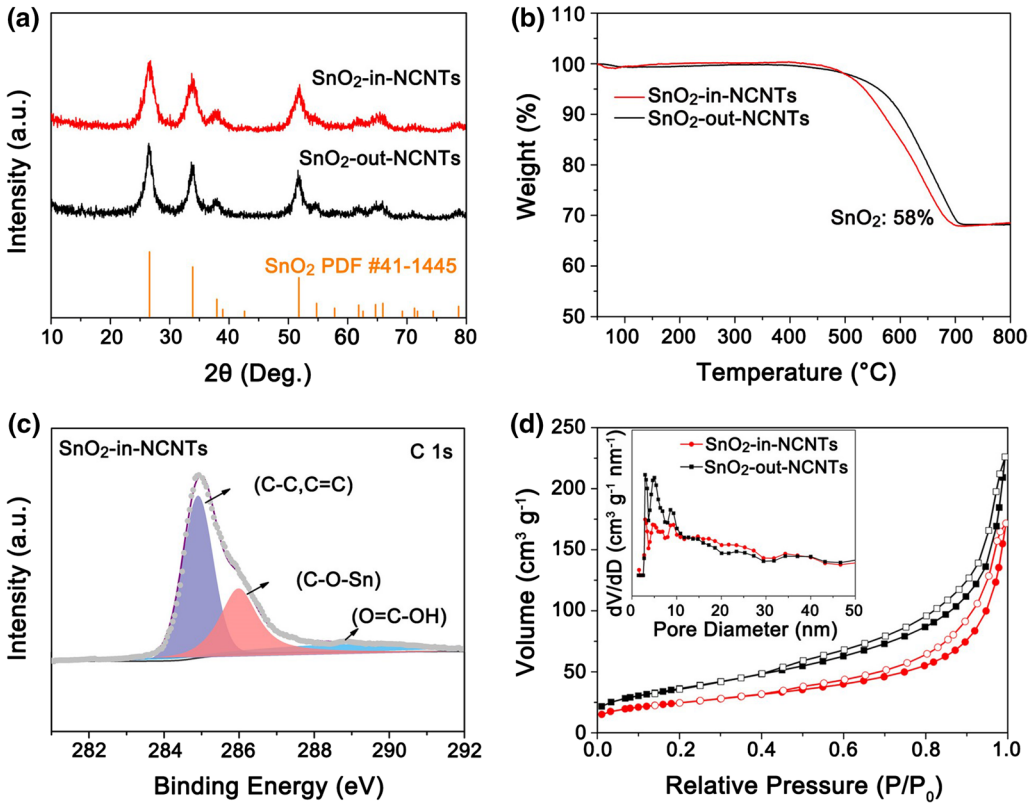

Fig. 3 (a) XRD pattern, (b) TG curves of the SnO_2-in-NCNTs and SnO_2-out-NCNTs, (c) C 1s XPS spectrum of SnO_2-in-NCNTs, (d) N_2 isotherms and pore-size distribution curves SnO_2-in-NCNTs and SnO_2-out-NCNTs.

The cycling performance at a current density of 0.2 A g^{-1} is displayed in Fig. S11, where the SnO_2-in-NCNTs enable a respectable capacity retention after 100 cycles. However, the SnO_2-out-NCNTs show an inferior cycling stability. Furthermore, the cycling performance of the electrode after 20 cycles of activation is shown in Fig. 4e. Even at a higher current density of 5 A g^{-1}, it still maintains a capacity of 483.6 mAh g^{-1} after 500 cycles. The CV measurement at various scan rates is studied to analyze the reaction kinetics (Fig. S12). At a scan rate of 1 mV s^{-1}, the capacitive contribution ratio of SnO_2-in-NCNTs is 64.5%. Benefitting from the fast capacitance-controlled lithium storage process, the SnO_2-in-NCNTs exhibit excellent fast charge–discharge capability.

The excellent electrochemical performance of the SnO_2-in-NCNTs electrodes can be attributed to the effective confined synthesis of SnO_2 nanoparticles in NCNTs. The advantages of such rationally designed structure are as follows: (1) The nitrogen doping in CNTs and V_O greatly improve the low electrical conductivity of SnO_2. (2) The 3D channel carbon skeleton structure cross-linked by NCNTs ensures the transport of ions and electrons, which are favorable for the excellent rate performance.[38] (3) Moreover, the confined space of NCNTs channels can restrict the particle size of SnO_2 and the sufficient void space in NCNTs can accommodate the large volume change during cycling. Therefore, the resultant electrode can effectively improve the poor kinetics of pure SnO_2 and maintain high structural integrity of the hybrids, resulting in high reversible capacities, superior rate capability and long cycle life.

In order to confirm the structural integrity associated with cyclic stability, we employed HRTEM measurement to explore the morphology change of SnO_2-in-NCNTs and SnO_2-out-NCNTs after 100 cycles at 0.2 A g^{-1}. As shown in Fig. 5a, the nanoparticles remain encapsulated within the tube in SnO_2-in-NCNTs. The fast Fourier transform (FFT) image (inset of Fig. 5a) matches well with the (110) and (211) facets of SnO_2. However, the SnO_2-out-NCNTs (Fig. 5b) suffers from particle agglomeration and pulverization. Figure S13 displays the EIS spectra of the two hybrids after cycles. The radius of SnO_2-in-NCNTs is smaller than SnO_2-out-NCNTs, which is mainly related to the cracking, exfoliation of SnO_2 and the thickening of the SEI film in the SnO_2-out-NCNTs during the cycling. Different structural evolutions of the two SnO_2-based hybrids can be better illustrated in Fig. 5c. When SnO_2 nanoparticles are embedded in the channel NCNTs, the NCNTs can effectively restrict the particle size of SnO_2 and accommodate

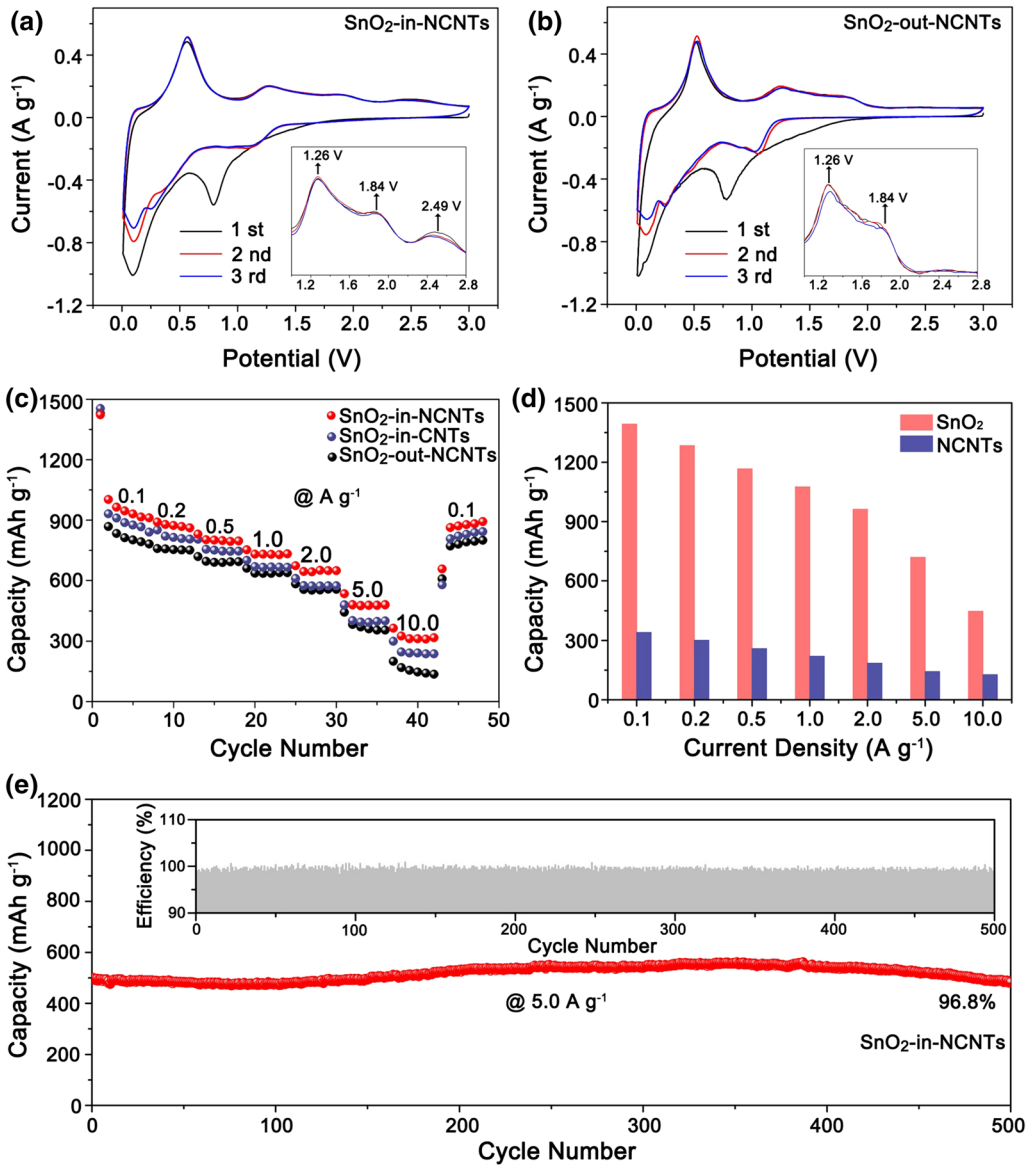

Fig. 4 (a-b) The CV curves of the SnO_2-in-NCNTs and SnO_2-out-NCNTs. (c) Rate performance at 0.1–10 A g^{-1} of the SnO_2-in-NCNTs, SnO_2-out-NCNTs and SnO_2-in-CNTs. (d) Capacity contributions of SnO_2 based on the values of NCNTs and SnO_2-in-NCNTs. (e) Cycling stability of the SnO_2-in-NCNTs at 5 A g^{-1}.

the volume expansion of SnO_2 during lithiation/delithiation processes. In addition, mechanical stress is relieved during cycling due to expansion along the available void space of the tube. Therefore, the design that SnO_2 encapsulated in carbon nanotubes can effectively stabilize the structural change and ensure a stable cycle ability.

Conclusion

In conclusion, the SnO_2-in-NCNTs with SnO_2 nanoparticles encapsulated in carbon nanotubes were successfully fabricated via capillary force. With the addition of PVP, the surface tension of the PVP/ethanol solution can be decreased, thus increasing the efficiency of capillary force. The introduction of V_O in SnO_2 and the highly conductive NCNTs can greatly improve electron transfer in the hybrids. In addition, the sufficient voids between particles can effectively alleviate volume expansion during the lithiation/delithiation processes. Moreover, the carbon nanotubes can assemble into interconnected networks, which is beneficial to the transfer of ions and electrons. As a result, the SnO_2-in-NCNTs demonstrate a superior cycling stability and high-rate capability. The capacity is well-maintained after 500 cycles at 5 A g^{-1} and the capacity can still reach 326.3 mAh g^{-1} even at 10 A g^{-1}. The present work opens up an

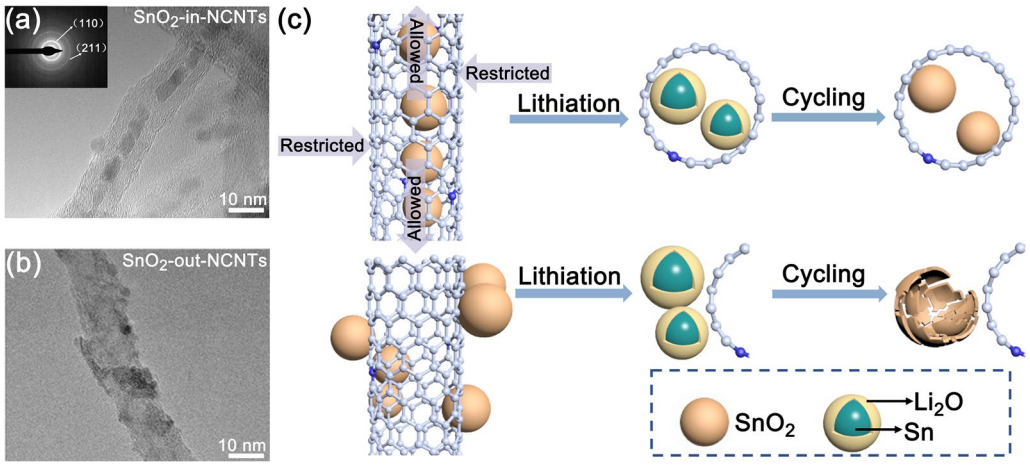

Fig. 5 (a-b) TEM image after 100 cycles at 0.2 A g^{-1} of the SnO_2-in-NCNTs and SnO_2-out-NCNTs. (c) Structural evolutions demonstration during lithiation/delithiation processes.

efficacious avenue to develop high-performance anode materials with encapsulated structure for LIBs.

Supplementary Information The online version contains supplementary material available at https://doi.org/10.1007/s11664-022-09975-z.

Acknowledgments This work was supported by the Innovation Program of Shanghai Municipal Education Commission and the Fundamental Research Funds for the Central Universities.

Conflict of interest The authors declare that they have no conflict of interest.

References

1. M. Armand and J.M. Tarascon, Building Better Batteries. *Nature* 451, 652 (2008).
2. L.A. Ellingsen, C.R. Hung, G. Majeau-Bettez, B. Singh, Z. Chen, M.S. Whittingham, and A.H. Stromman, Nanotechnology for Environmentally Sustainable Electromobility. *Nat. Nanotechnol.* 11, 1039 (2016).
3. G. Derrien, J. Hassoun, S. Panero, and B. Scrosati, Nanostructured Sn-C Composite as an Advanced Anode Material in High-Performance Lithium-Ion Batteries. *Adv. Mater.* 19, 2336 (2007).
4. X.Y. Li, Y.M. Chen, H.T. Wang, H.M. Yao, H.T. Huang, Y.W. Mai, N. Hu, and L.M. Zhou, Inserting Sn Nanoparticles into the Pores of TiO_{2-x}-C Nanofibers by Lithiation. *Adv. Funct. Mater.* 26, 376 (2016).
5. K. Ma, Y. Liu, H. Jiang, Y.J. Hu, R. Si, H.L. Liu, and C.Z. Li, Multivalence-Ion Intercalation Enables Ultrahigh 1T Phase MoS_2 Nanoflowers to Enhanced Sodium-Storage Performance. *CCS Chem.* 2, 1472 (2020).
6. Y.R. Dong, Yu. Liu, Y.J. Hu, K. Ma, H. Jiang, and C.Z. Li, Boosting Reaction Kinetics and Reversibility in Mott-Schottky VS_2/MoS_2 Heterojunctions for Enhanced Lithium Storage. *Sci. Bull.* 65, 1470 (2020).
7. J.G. Zhu, D.L. Chao, W.L. Xu, M.H. Wu, and H.J. Zhang, Microscale Si-based Anodes: Fundamental Understanding and Industrial Prospects for Practical High-energy Lithium-Ion Batteries. *ACS Nano* 15, 15567 (2021).
8. C. Hu, Y.J. Hu, A.P. Chen, X.Z. Duan, H. Jiang, and C.Z. Li, Atomic Interface Catalytically Synthesizing SnP/CoP Hetero-Nanocrystals within Dual-Carbon Hybrids for Ultrafast Lithium-Ion Batteries. *Engineering* (2022). https://doi.org/10.1016/j.eng.2021.11.026.
9. Y. Liu, C. Hu, L. Chen, Y.J. Hu, H. Jiang, and C.Z. Li, Confining Ultrahigh Oxygen Vacancy SnO_2 Nanocrystals into Nitrogen-Doped Carbon for Enhanced Li-Ion Storage Kinetics and Reversibility. *J. Energy. Chem.* 69, 450 (2022).
10. C. Hu, L. Chen, Y.J. Hu, A.P. Chen, L. Chen, H. Jiang, and C.Z. Li, Light-Motivated SnO_2/TiO_2 Heterojunctions Enabling the Breakthrough in Energy Density for Lithium-Ion Batteries. *Adv. Mater.* 33, 2103558 (2021).
11. C. Hu, L. Chen, Y.J. Hu, A.P. Chen, L. Chen, H. Jiang, and C.Z. Li, Optimizing SnO_{2-x}/Fe_2O_3 Hetero-Nanocrystals Toward Rapid and Highly Reversible Lithium Storage. *Small* 17, 2103532 (2021).
12. H.B. Wu, J.S. Chen, H.H. Hng, and X. Wen Lou, Nanostructured Metal Oxide-Based Materials as Advanced Anodes for Lithium-Ion Batteries. *Nanoscale* 4, 2526 (2012).
13. D. Larcher, S. Beattie, M. Morcrette, K. Edstroem, J.C. Jumas, and J.M. Tarascon, Recent Findings and Prospects in the Field of Pure Metals as Negative Electrodes for Li-Ion Batteries. *J. Mater. Chem.* 17, 3759 (2007).
14. P. Meduri, C. Pendyala, V. Kumar, G.U. Sumanasekera, and M.K. Sunkara, Hybrid Tin Oxide Nanowires as Stable and High Capacity Anodes for Li-Ion Batteries. *Nano Lett.* 9, 612 (2009).
15. H.P. Cong, S. Xin, and S.H. Yu, Flexible Nitrogen-Doped Graphene/SnO_2 Foams Promise Kinetically Stable Lithium Storage. *Nano Energy* 13, 482 (2015).
16. W.S. Kim, Y. Hwa, J.H. Jeun, H.J. Sohn, and S.H. Hong, Synthesis of SnO_2 Nano Hollow Spheres and Their Size Effects in Lithium Ion Battery Anode Application. *J. Power Sources* 225, 108 (2013).
17. P. Wu, N. Du, H. Zhang, J. Yu, and D. Yang, CNTs@SnO_2@C Coaxial Nanocables with Highly Reversible Lithium Storage. *J. Phys. Chem. C* 114, 22535 (2010).
18. D. Wang, J. Yang, X. Li, D. Geng, R. Li, M. Cai, T.K. Sham, and X. Sun, Layer by Layer Assembly of Sandwiched Graphene/SnO_2 Nanorod/Carbon Nanostructures with Ultrahigh Lithium Ion Storage Properties. *Energy Environ. Sci.* 6, 2900 (2013).

19. X.S. Zhou, Z.H. Dai, S.H. Liu, J.C. Bao, and Y.G. Guo, Ultra-Uniform SnO_x/Carbon Nanohybrids toward Advanced Lithium-Ion Battery Anodes. *Adv. Mater.* 26, 3943 (2014).
20. C.R. Ma, W.M. Zhang, Y.S. He, Q. Gong, H.Y. Che, and Z.F. Ma, Carbon coated SnO_2 Nanoparticles Anchored on CNT as A Superior Anode Material for Lithium-ion Batteries. *Nanoscale* 8, 4121 (2016).
21. C.H. Xu, J. Sun, and L. Gao, Synthesis of Multiwalled Carbon Nanotubes That Are Both Filled and Coated by SnO_2 Nanoparticles and Their High Performance in Lithium-Ion Batteries. *J. Phys. Chem. C* 113, 47 (2009).
22. M. Liu, S. Zhang, H.C. Dong, X. Chen, S. Gao, Y.P. Sun, W.H. Li, J.Q. Xu, L.W. Chen, A.B. Yuan, and W. Lu, Nano-SnO_2/Carbon Nanotube Hairball Composite as a High-Capacity Anode Material for Lithium Ion Batteries. *ACS Sust. Chem. Eng.* 7, 4195 (2019).
23. Y.J. Chen, C.L. Zhu, and T.H. Wang, The Enhanced Ethanol Sensing Properties of Multi-Walled Carbon Nanotubes/SnO_2 Core/Shell Nanostructures. *Nanotechnology* 17, 3012 (2006).
24. E. Dujardin, T.W. Ebbesen, H. Hiura, and K. Tanigaki, Capillarity and Wetting of Carbon Nanotubes. *Science* 265, 1850 (1994).
25. P.M. Ajayan, and S. Iijima, Capillarity-Induced Filling of Carbon Nanotubes. *Nature* 361, 333 (1993).
26. H.P. Guo, B.Y. Ruan, L.L. Liu, L. Zhang, Z.L. Tao, S.L. Chou, J.Z. Wang, and H.K. Liu, Capillary-Induced Ge Uniformly Distributed in N-doped Carbon Nanotubes with Enhanced Li-Storage Performance. *Small* 13, 1700920 (2017).
27. R. Jia, J.L. Yue, Q.Y. Xia, J. Xu, X.H. Zhu, S. Sun, T. Zha, and H. Xia, Carbon Shelled Porous $SnO_{2-\delta}$ Nanosheet Arrays as Advanced Anodes for Lithium-Ion Batteries. *Energy Storage Mater.* 13, 303 (2018).
28. L. Sun, H.C. Si, Y.X. Zhang, Y. Shi, K. Wang, J.G. Liu, and Y.H. Zhang, Sn-SnO_2 Hybrid Nanoclusters Embedded in Carbon Nanotubes with Enhanced Electrochemical Performance for Advanced Lithium Ion Batteries. *J. Power Sources* 415, 126 (2019).
29. C. Weidenthaler, A.H. Lu, W. Schmidt, and F. Schüth, X-ray Photoelectron Spectroscopic Studies of PAN-Based Ordered Mesoporous Carbons (OMC). *Micropor. Mesopor. Mater.* 88, 238 (2006).
30. Z.T. Li, Y.F. Dong, J.Z. Feng, T. Xu, H. Ren, C. Gao, Y.R. Li, M.J. Cheng, W.T. Wu, and M.B. Wu, Controllably Enriched Oxygen Vacancies through Polymer Assistance in Titanium Pyrophosphate as a Super Anode for Na/K-Ion Batteries. *ACS Nano* 13, 9227 (2019).
31. B. Liu, S. Sun, R.Y. Jia, H.S. Zhang, X.H. Zhu, C.G. Zhang, J. Xu, T. Zhai, and H. Xia, Oxygen-Deficient Homo-Interface toward Exciting Boost of Pseudocapacitance. *Adv. Funct. Mater.* 30, 1909546 (2020).
32. Q.M. Gan, H.N. He, K.M. Zhao, Z. He, S.Q. Liu, and S.P. Yang, Plasma-Induced Oxygen Vacancies in Urchin-Like Anatase Titania Coated by Carbon for Excellent Sodium-Ion Battery Anodes. *ACS Appl. Mater. Interfaces* 10, 7031 (2018).
33. L.L. Liu, M.Z. An, P.X. Yang, and J.Q. Zhang, Superior Cycle Performance and High Reversible Capacity of SnO_2/Graphene Composite as an Anode Material for Lithium-ion Batteries. *Sci. Rep.* 5, 9055 (2015).
34. J. Qin, C.N. He, N.Q. Zhao, Z.Y. Wang, C.S. Shi, E.Z. Liu, and J.J. Li, Graphene Networks Anchored with Sn@Graphene as Lithium Ion Battery Anode. *ACS Nano* 8, 1728 (2014).
35. X.Y. Shan, Y. Zhong, L.J. Zhang, Y.Q. Zhang, X.H. Xia, X.L. Wang, and J.P. Tu, A Brief Review on Solid Electrolyte Interphase Composition Characterization Technology for Lithium Metal Batteries: Challenges and Perspectives. *J. Phys. Chem. C* 125, 19060 (2021).
36. H.G. Wang, Q. Wu, Y.H. Wang, X. Wang, L.L. Wu, S.Y. Song, and H.J. Zhang, Molecular Engineering of Monodisperse SnO_2 Nanocrystals Anchored on Doped Graphene with High-Performance Lithium/Sodium-Storage Properties in Half/Full Cells. *Adv. Energy Mater.* 9, 1802993 (2019).
37. C.H. Wang, Y.H. Li, F. Cao, Y.Q. Zhang, X.H. Xia, and L.J. Zhang, Employing Ni-Embedded Porous Graphitic Carbon Fibers for High Efficiency Lithium-Sulfur Batteries. *ACS Appl. Mater. Interfaces* 14, 10457 (2022).
38. Z.Y. Pan, J. Ren, G.Z. Guan, X. Fang, B.J. Wang, S.G. Doo, I.H. Son, X.L. Huang, and H.S. Peng, Synthesizing Nitrogen-Doped Core-Sheath Carbon Nanotube Films for Flexible Lithium Ion Batteries. *Adv. Energy Mater.* 6, 1600271 (2016).